J Periodontal Implant Sci. 2016 Oct;46(5):303-319
https://doi.org/10.5051/jpis.2016.46.5.303
pISSN 2093-2278·eISSN 2093-2286

JPIS
Journal of Periodontal & Implant Science

Research Article

Check for updates

The influence of root surface distance to alveolar bone and periodontal ligament on periodontal wound healing

Marco Montevecchi,[1,*] Annapaola Parrilli,[2] Milena Fini,[3] Maria Rosaria Gatto,[1] Aurelio Muttini,[4] Luigi Checchi[1]

[1]Division of Periodontology and Implantology, Department of Biomedical and Neuromotor Sciences, Alma Mater Studiorum, University of Bologna School of Dentistry, Bologna, Italy
[2]BITTA Laboratory, Rizzoli Orthopaedic Institute, Bologna, Italy
[3]Preclinical and Surgical Studies Laboratory, Rizzoli Orthopaedic Institute, Bologna, Italy
[4]Faculty of Veterinary Medicine, Teramo University, Teramo, Italy

Received: Apr 29, 2016
Accepted: Jul 28, 2016

***Correspondence to**
Marco Montevecchi
Division of Periodontology and Implantology, Department of Biomedical and Neuromotor Sciences, Alma Mater Studiorum, University of Bologna School of Dentistry, Via San Vitale 59, Bologna 40100, Italy.
E-mail: m.montevecchi@unibo.it
Tel: +39-51-2088156
Fax: +39-51-225208

ORCID
Marco Montevecchi
http://orcid.org/0000-0001-7312-802X
Annapaola Parrilli
http://orcid.org/0000-0003-0251-5094
Milena Fini
http://orcid.org/0000-0002-3732-3570
Maria Rosaria Gatto
http://orcid.org/0000-0003-0216-9056
Aurelio Muttini
http://orcid.org/0000-0002-2133-4144
Luigi Checchi
http://orcid.org/0000-0002-2578-3983

ABSTRACT

Purpose: The purpose of this animal study was to perform a 3-dimensional micro-computed tomography (micro-CT) analysis in order to investigate the influence of root surface distance to the alveolar bone and the periodontal ligament on periodontal wound healing after a guided tissue regeneration (GTR) procedure.
Methods: Three adult *Sus scrofa domesticus* specimens were used. The study sample included 6 teeth, corresponding to 2 third mandibular incisors from each animal. After coronectomy, a circumferential bone defect was created in each tooth by means of calibrated piezoelectric inserts. The experimental defects had depths of 3 mm, 5 mm, 7 mm, 9 mm, and 11 mm, with a constant width of 2 mm. One tooth with no defect was used as a control. The defects were covered with a bioresorbable membrane and protected with a flap. After 6 months, the animals were euthanised and tissue blocks were harvested and preserved for micro-CT analysis.
Results: New alveolar bone was consistently present in all experimental defects. Signs of root resorption were observed in all samples, with the extent of resorption directly correlated to the vertical extent of the defect; the medial third of the root was the most commonly affected area. Signs of ankylosis were recorded in the defects that were 3 mm and 7 mm in depth. Density and other indicators of bone quality decreased with increasing defect depth.
Conclusions: After a GTR procedure, the periodontal ligament and the alveolar bone appeared to compete in periodontal wound healing. Moreover, the observed decrease in bone quality indicators suggests that intrabony defects beyond a critical size cannot be regenerated. This finding may be relevant for the clinical application of periodontal regeneration, since it implies that GTR has a dimensional limit.

Keywords: Bone and bones; Guided tissue regeneration; Three-dimensional imaging; Periodontium; Research design; Root resorption

Conflict of Interest
No potential conflict of interest relevant to this article was reported.

INTRODUCTION

The goal of periodontal therapy is to arrest the progression of disease, to restore the damaged periodontal apparatus, and to prevent the recurrence of disease, maintaining healthy and comfortable natural dentition [1,2].

Preclinical and clinical studies have conclusively shown that many histological features associated with periodontal restoration can be confirmed after periodontal therapy [3-5].

Two distinct terms are conventionally used to define this concept: repair and regeneration. The former indicates the healing of wound tissue that does not fully restore the architecture and function of the affected region, while the latter refers to the reconstruction of a lost or injured area. According to these definitions, periodontal regeneration results in a completely new and exact duplicate of the lost periodontium, including well-oriented collagen fibres, alveolar bone, and cementum [2,3,6].

Regeneration must be explained with close reference to the complex interactions among the different tissues involved. Findings from experimental studies have clearly shown that during periodontal wound healing, cells from 4 different areas compete for repopulation of the site: oral epithelium, gingival connective tissue, bone, and periodontal ligament. If the oral epithelium arrives to the tooth surface before the other tissues, the result will be a long junctional epithelium. If the cells from the gingival connective tissue are the first to repopulate the area, the result will be a group of connective tissue fibres parallel to the tooth surface, remodelling the alveolar bone with no attachment to the cementum. External resorption may occur. If bone cells are allowed to repopulate the area, root resorption (RR), and ankylosis may occur. Finally, when only the cells from the periodontal ligament proliferate coronally, newly formed cementum, and periodontal ligament will emerge [6-9].

Therefore, the residual periodontal ligament plays a crucial role in periodontal regeneration, due to the ability of the inner stromal cells to restore cementum, bone, and the periodontal ligament [10,11].

Since the epithelium and gingival connective tissue are known to exhibit faster repopulation of a wound, one of the main goals of periodontal regenerative therapy is to prevent their apical proliferation [12,13].

Guided tissue regeneration (GTR) involves the use of a barrier membrane to prevent the downward growth of these tissues, leaving bone, and the periodontal ligament to self-regulate [14-16].

Since alveolar bone and the periodontal ligament have shown similar developmental timing during the healing process [17,18], it can be speculated that the initial distance from these tissues to the root surface may play a crucial role in the final result.

The present study investigates, after a GTR procedure, the null hypothesis that the distance of the periodontal ligament and alveolar bone to the root surface does not influence the periodontal wound healing process. Artificial periodontal defects on animal models were surgically created and analysed using 3-dimensional micro-computed tomography (micro-CT) after 6 months of healing.

https://doi.org/10.5051/jpis.2016.46.5.303

MATERIALS AND METHODS

The study was conducted in compliance with the Italian animal welfare guidelines (authorisation request, protocol no. 414 submitted on July 2, 2009).

Three adult *Sus scrofa domesticus* specimens (age, 18 months) weighing 60–90 kg were used in this study. This mammalian species, which potentially suffers from periodontal disease [19], it is considered a clinically relevant experimental model [20]. The tooth chosen for the study was the third mandibular incisor, a single-rooted tooth characterized by the absence of continuous eruption.

The study sample included 6 teeth, with 2 teeth drawn from each animal. The allocation was randomly assigned (Table 1).

Surgical procedures and tissue preparation

Surgical procedures were performed under general anaesthesia (0.2 mg/kg of intravenous diazepam and 6 mg/kg of intravenous ketamine) and local anaesthesia (Mepivacaina® 3%+Adrenalin 5 mg/mL, AstraZeneca, Milano, Italy).

Following an intracrevicular incision, buccal, and lingual full-thickness flaps were raised around the teeth included in the experiment. Vertical incisions were made on the facial surface to permit the apical positioning of the flap. The tooth crown was removed at the highest level of the alveolar crest with a bur in a high-speed hand piece using a sterile water spray; root canal therapy was not performed. Sharp edges of the roots were rounded with a finishing bur.

After the coronectomy, a circumferential defect was created on each tooth, while one tooth was used as a control and had no defect. A width of 2 mm was maintained, while defects 3 mm, 5 mm, 7 mm, 9 mm, and 11 mm in depth were made in the 5 experimental teeth (Figure 1).

A circumferential intrabony defect was produced using a piezoelectric surgical device (Piezosurgery®, Mectron s.p.a., Genova, Italy). A sequence of specific inserts was used: an OP6 insert for the initial pilot osteotomy, root debridement, and root planning; an OT4 for micrometric osteotomy; and an OT5 to finalize the osteotomy and for the apical notch. During the procedure, the cementum layer of each root was removed from the coronal cut surface to the marginal level of the supporting alveolar bone. A bioresorbable membrane (Bio-Guide, Geistlich, Princeton, NJ, USA) was placed on the treated area, and then completely covered by a coronally displaced flap. Internal resorbable mattress sutures were performed (Vicryl 3.0, Ethicon Inc., Somerville, NJ, USA). After surgery, the animals were administered antibiotics daily for 3 days (penicillin G, 200,000 units) and housed in an open space with a stock diet and tap water available *ad libitum*. Analgesic/anti-inflammatory therapy

Table 1. Study sample description: allocation of the experimental defect depths and comparative control on the third mandibular incisors

Animal code	Tooth side	Defect depth (mm)
1	Right	-
2	Left	3
3	Right	5
3	Left	7
2	Right	9
1	Left	11

https://doi.org/10.5051/jpis.2016.46.5.303

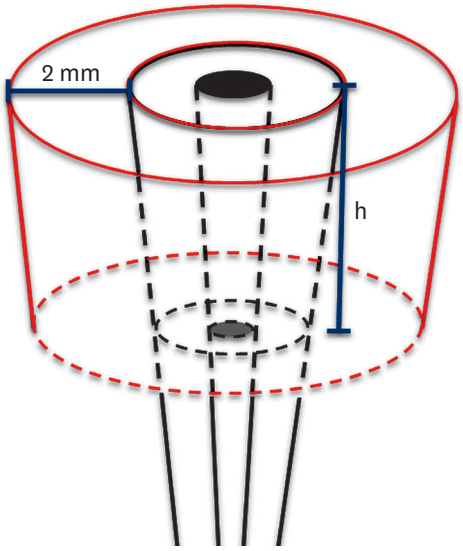

Figure 1. Scheme of the circumferential defects with constant distance (2 mm) between the root surface and bone margin and with increasing depth (h) depending on sample (h=3, 5, 7, 9, or 11 mm).

(2.2 mg/kg of intramuscular flunixin meglumine once per day for 3 days) was administered for pain control.

After 6 months of healing, the animals were sacrificed with an overdose of pentothal-sodium solution.

The mandibles were removed, and tissue blocks containing the experimental teeth were harvested and maintained at −20°C.

Micro-computed tomography analysis

For quantitative 3-dimensional (3D) analysis of the alveolar bone defects, the specimens were scanned using a high-resolution micro-CT system (SkyScan 1172, Bruker Micro-CT, Kontich, Belgium).

The X-ray generator was operated at a voltage of 100 kV with a current of 100 μA, and an aluminium filter 0.5 mm in thickness was placed between the sample and X-ray source. Each sample was rotated 180° with rotation steps of 0.4° and a nominal resolution of 6 μm (pixel size). The images obtained were later reconstructed using NRecon version 1.6.8 (Bruker Micro-CT) with beam hardening, ring artefact corrections, and specific post-alignment settings. The datasets consisted of images in an 8-bit '.jpg' format (4,000×4,000 pixels, with a 6 μm pixel size in all 3 spatial dimensions).

Preliminary micro-CT analysis of periodontal ligament width in the control tooth

The specimen was oriented according to the axis of the tooth, and a volume of interest (VOI) of 5×5 mm with a height of 12 mm was selected, including the periodontal ligament and the alveolar bone between the control tooth and the adjacent tooth. The height of 12 mm was selected since the maximum defect depth was 11 mm. The width of the periodontal ligament was measured within the VOI in 3D, and was defined as the empty space between the root and alveolar bone. Linear measurements (mm) of the periodontal space of the control tooth were taken to establish its average width, which was found to be 0.4 mm.

https://doi.org/10.5051/jpis.2016.46.5.303

Volumetric micro-CT analysis

After determining that the average width of the periodontal ligament in the pigs was 0.4 mm, the bone volume of the five experimental teeth and the control tooth was measured.

Since the width of the experimental defects was 2 mm and that the width of the periodontal ligament was 0.4 mm, we divided the defect space (2 mm) into 5 smaller areas measuring 0.4 mm each. We then calculated the amount of regenerated bone in each of those areas, following the following classification: A1, ≤0.4 mm; A2, 0.4–0.8 mm; A3, 0.8–1.2 mm; A4, 1.2–1.6 mm; A5, 1.6–2.0 mm.

Quantitative 3D distribution analyses were carried out using CTAn version 1.13 (Bruker Micro-CT). The specific VOIs were defined in each sample according to the small areas defined above and using a height of 12 mm. All five VOIs were further divided vertically along the tooth root axis into coronal, medial, and apical thirds, proportionally to the VOI height (4 mm for each third).

In the alveolar bone and root areas, 3D parameters were calculated in order to evaluate morphological changes due to the surgically created artificial periodontal defect. Bone density (BV/TV) was defined as the ratio between the volume of bone within the VOI and the total volume of the VOI and was calculated as a percentage. The trabecular thickness (Tb.Th) of the alveolar bone was calculated in millimetres using the model described by Hildebrand and Rüegsegger [21] over the total volume of the VOI. The trabecular number (Tb.N), defined as the number of intersections through a trabecular structure per unit length of a random linear path through the VOI, was calculated in mm^{-1}. The trabecular separation (Tb.Sp) was calculated in millimetres in the same way as the Tb.Th. In addition, bone-root contact (BRC) was defined as the intersection of the root and alveolar bone surfaces intersection and calculated in millimetres squared, and RR was defined as the volume of root damage and calculated in millimetres cubed.

Statistical analysis

A generalized linear mixed effect model was used to evaluate the effects of defect depth, area, and the interaction between these two fixed factors on the parameters related to the bone structure overall and in the coronal third of the VOI. Plotting the observed vs. estimated values of BV/TV, Tb.Th, Tb.N, and Tb.Sp, a good linear fit of the data to the model was observed. The alpha level was set a priori at 0.05. When multiple comparisons among areas were performed, A5 was considered the reference area due to its proximity to the bone.

According to the suggestion of Russell and Burch [22] regarding reduction of the animal number, the sample size was calculated for a split-mouth design with a power of 80% and an alpha level of 0.05 for a two-sided test, using the results of BV/TV (%) derived from the present study for each area as the main outcome, except for A1, which hypothetically corresponded to the periodontal ligament.

RESULTS

The healing phase was uneventful and none of the experimental teeth penetrated the soft tissue covering, resulting in exposure to the oral cavity.

https://doi.org/10.5051/jpis.2016.46.5.303

JPIS Journal of Periodontal & Implant Science

Quantitative analysis

The results of micro-CT analysis of the regenerated bone according to samples and areas are summarized in Figure 2 and Table 2.

BV/TV significantly decreased with increased defect depth and differed significantly among the areas (P=0.001). In particular, it was higher in A2, A3, and A4 than in A5.

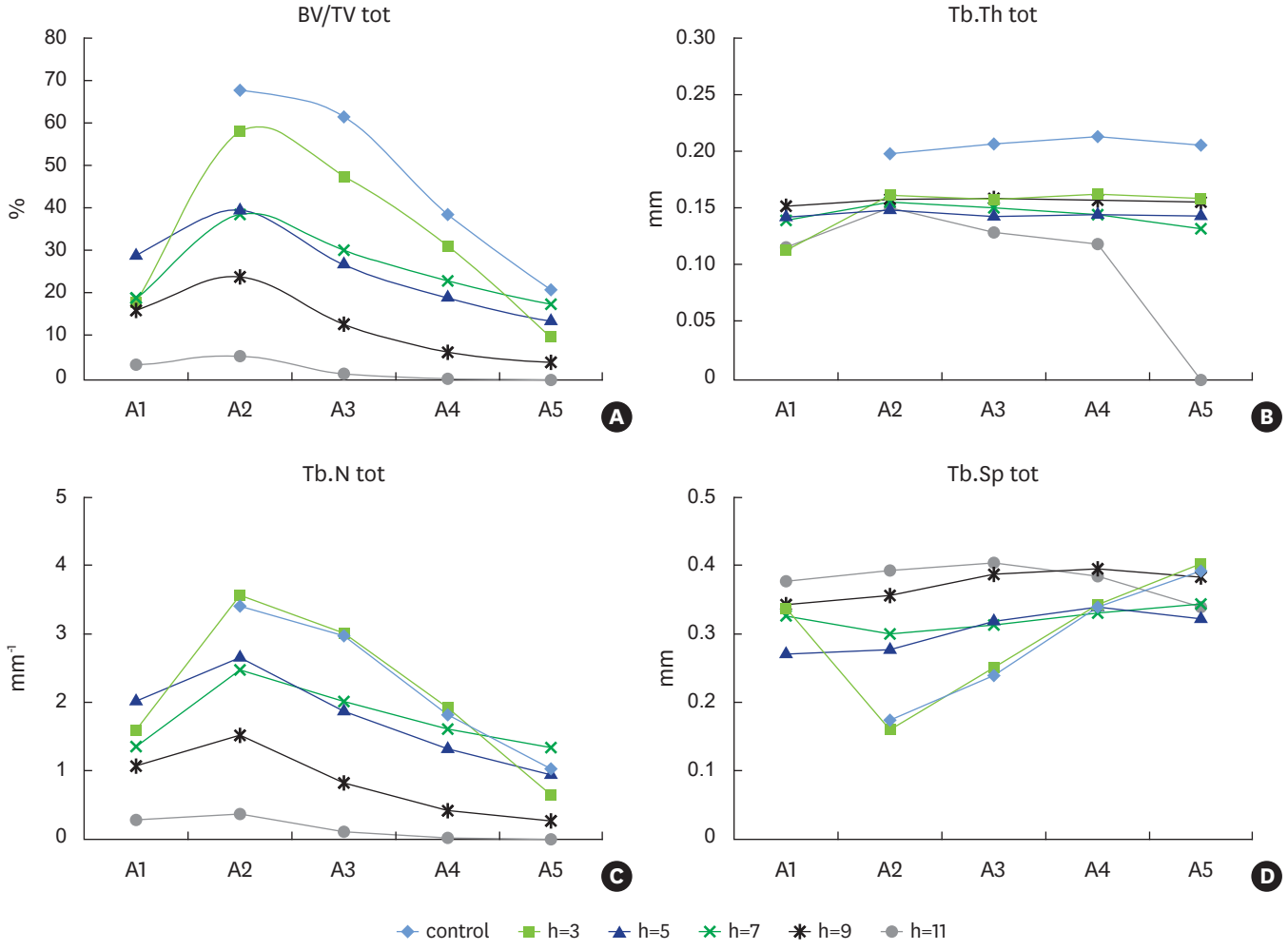

Figure 2. Microstructure bone parameters of alveolar bone along the entire height (h) of the defect (12 mm) but at the different area distance from the root (i.e., A1 at ≤0.4 mm, A2 at 0.4–0.8 mm, A3 at 0.8–1.2 mm, A4 at 1.2–1.6 mm, A5 at 1.6–2.0 mm). (A) Values of bone density (BV/TV) in %; (B) values of trabecular thickness (Tb.Th) in mm; (C) values of trabecular number (Tb.N) in mm^{-1}; (D) values of trabecular separation (Tb.Sp) in mm for all samples including control.

Table 2. Generalized linear model results relative to the total tooth. Outcome measurements (P values) are reported among areas using area 5 as a reference

Total	BV/TV	Tb.Th	Tb.Sp	Tb.N
Akaike criterion	166.996	−49.840	−30.404	63.673
Corrected model	0.001	0.003	0.001	0.001
Depth	0.001	0.020	0.001	0.001
Area	0.001	0.002	0.001	0.001
Interaction of depth and area	0.001	0.005	0.007	0.012
Area 1	0.385	0.001	0.001	0.902
Area 2	0.001	0.327	0.001	0.001
Area 3	0.001	0.424	0.007	0.001
Area 4	0.017	0.571	0.267	0.084

BV/TV, bone density; Tb.Th, trabecular thickness; Tb.Sp, trabecular separation; Tb.N, trabecular number.

https://doi.org/10.5051/jpis.2016.46.5.303

Tb.Th significantly decreased with increased defect depth (P=0.020) and differed significantly among the areas (P=0.002); the Tb.Th values showed a general decrease in the experimental teeth in comparison to the control values and were very similar except for A5 in the tooth with an 11-mm defect.

Tb.Sp significantly increased with increased defect depth and differed significantly among the areas (P=0.001). In particular, it was significantly higher in A1, A2, and A3 than in A5.

Tb.N significantly decreased with increased defect depth and differed significantly among the areas (P=0.001). In particular, it was significantly higher in A2 and A3 than in A5.

Since the experimental defects ranged between 3 mm and 11 mm, we decided to focus on the coronal portion of each specimen in order to account primarily for the healed bone. Data on the bone structure of the coronal third are presented in Figure 3 and Table 3.

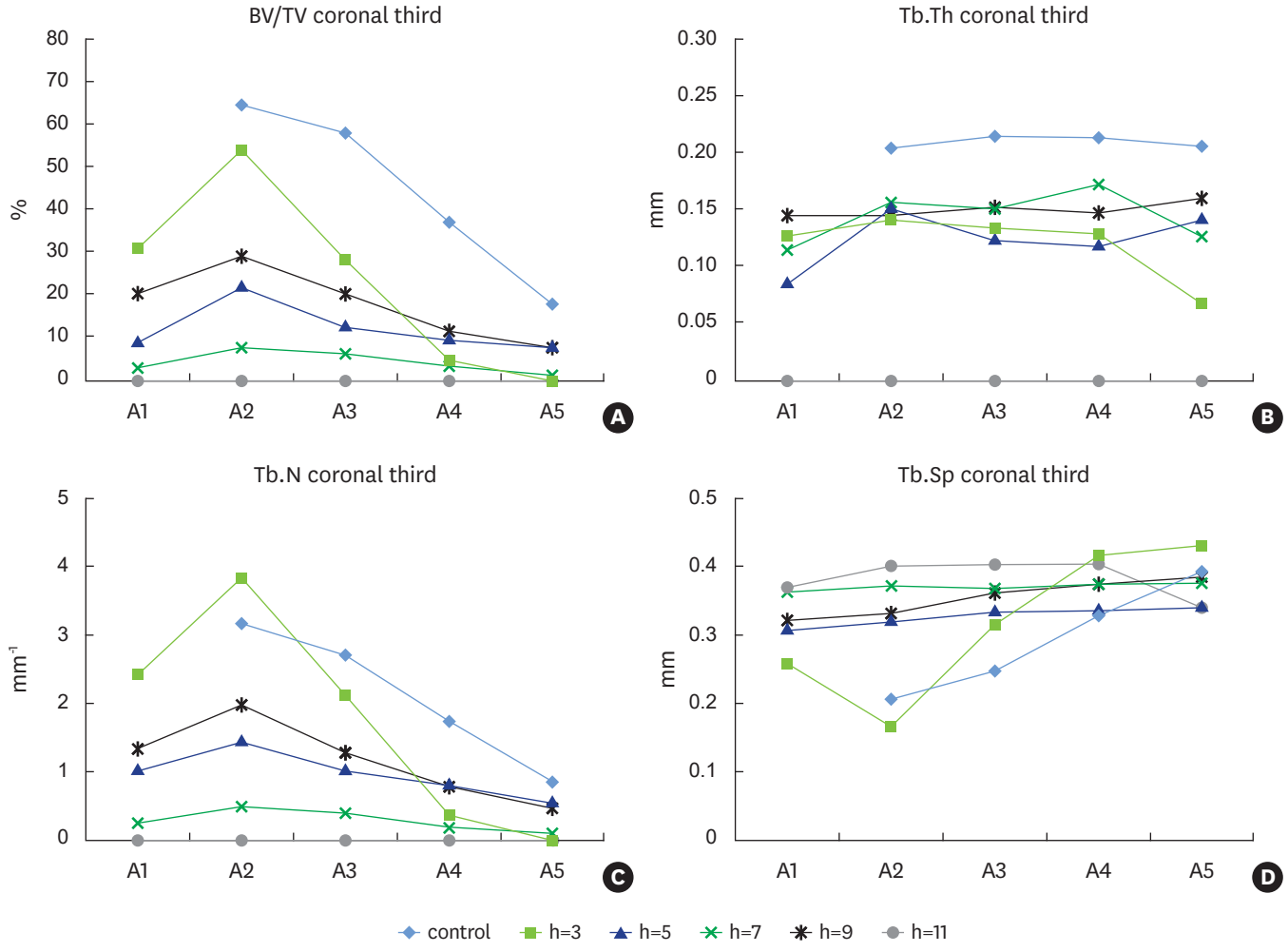

Figure 3. Microstructure bone parameters of alveolar bone at the coronal thirds and at the different area distance from the root (i.e., A1 at ≤0.4 mm, A2 at 0.4–0.8 mm, A3 at 0.8–1.2mm, A4 at 1.2–1.6 mm, A5 at 1.6–2.0 mm). (A) Values of bone density (BV/TV) in %; (B) values of trabecular thickness (Tb.Th) in mm; (C) values of trabecular number (Tb.N) in mm^{-1}; (D) values of trabecular separation (Tb.Sp) in mm for all samples including control.
h, height.

https://doi.org/10.5051/jpis.2016.46.5.303

Table 3. Generalized linear model results among areas relative to the coronal third. Outcome measurements (*P* values) are reported among areas using area 5 as a reference

Coronal third	BV/TV	Tb.Th	Tb.Sp	Tb.N
Akaike criterion	188.754	−25.555	−30.078	76.488
Corrected model	0.001	0.003	0.001	0.004
Depth	0.001	0.004	0.001	0.001
Area	0.004	0.209	0.001	0.015
Interaction of depth and area	0.072	0.502	0.006	0.200
Area 1	0.911	0.128	0.001	0.743
Area 2	0.010	0.593	0.001	0.003
Area 3	0.017	0.640	0.019	0.049
Area 4	0.340	0.660	0.315	0.611

BV/TV, bone density; Tb.Th, trabecular thickness; Tb.Sp, trabecular separation; Tb.N, trabecular number.

BV/TV generally decreased as the size of the defect increased (P=0.001) and differed significantly among the areas (P=0.004). Particularly significant differences were observed in the BV/TV of A2 and A3 vs. A5 for each defect depth. A2 showed the highest BV/TV values for all the samples, except for the tooth with an 11-mm defect.

Tb.Th sequentially decreased with increasing defect depth (P=0.004), except for the teeth with 7-mm and 9-mm defects.

Tb.Sp values generally increased with increasing defect depth (P=0.001). When compared to the control, Tb.Sp values were higher in all experimental samples and in all areas, A5 excluded, except for the experimental tooth with a 3-mm defect. In particular, it was significantly higher in A1, A2, and A3 than in A5.

Tb.N sequentially decreased with increasing defect depths (P=0.001), except for the tooth with a 5-mm defect. The influence of area was significant (P=0.015); particularly significant differences were observed in A2 and A3 vs. A5 for each defect depth. A2 always presented higher values than the other areas.

Microstructural observations of the coronal portion showed results similar to those observed in the overall samples.

No quantitative analysis was performed for BRC or RR due to the paucity of data.

Qualitative analysis

With regard to the bone parameters BV/TV and Tb.Th, 3D models of the alveolar bone along the entire height of the defect were created and coloured according to a colour-coded RGB scale for thickness. The coloured models in the different areas reflecting increasing distances from the root (A1, A2, etc.) are shown in Figure 4. The 3D thickness measurement method is referred to as sphere-fitting thickness, and is locally defined as the diameter of the largest enclosed sphere providing a visual representation of how the thickness of the structure is distributed throughout the samples. The images of the bone indicate the quantity and the quality of the alveolar bone in various areas and agree with the BV/TV and Tb.Th results shown in Figures 2 and 3.

RR and alveolar BRC (ankyloses) are described and shown in Figure 5. RR showed increasing values with increasing height of the defect. Areas without signs of RR were also found. For

https://doi.org/10.5051/jpis.2016.46.5.303

JPIS
Journal of Periodontal & Implant Science

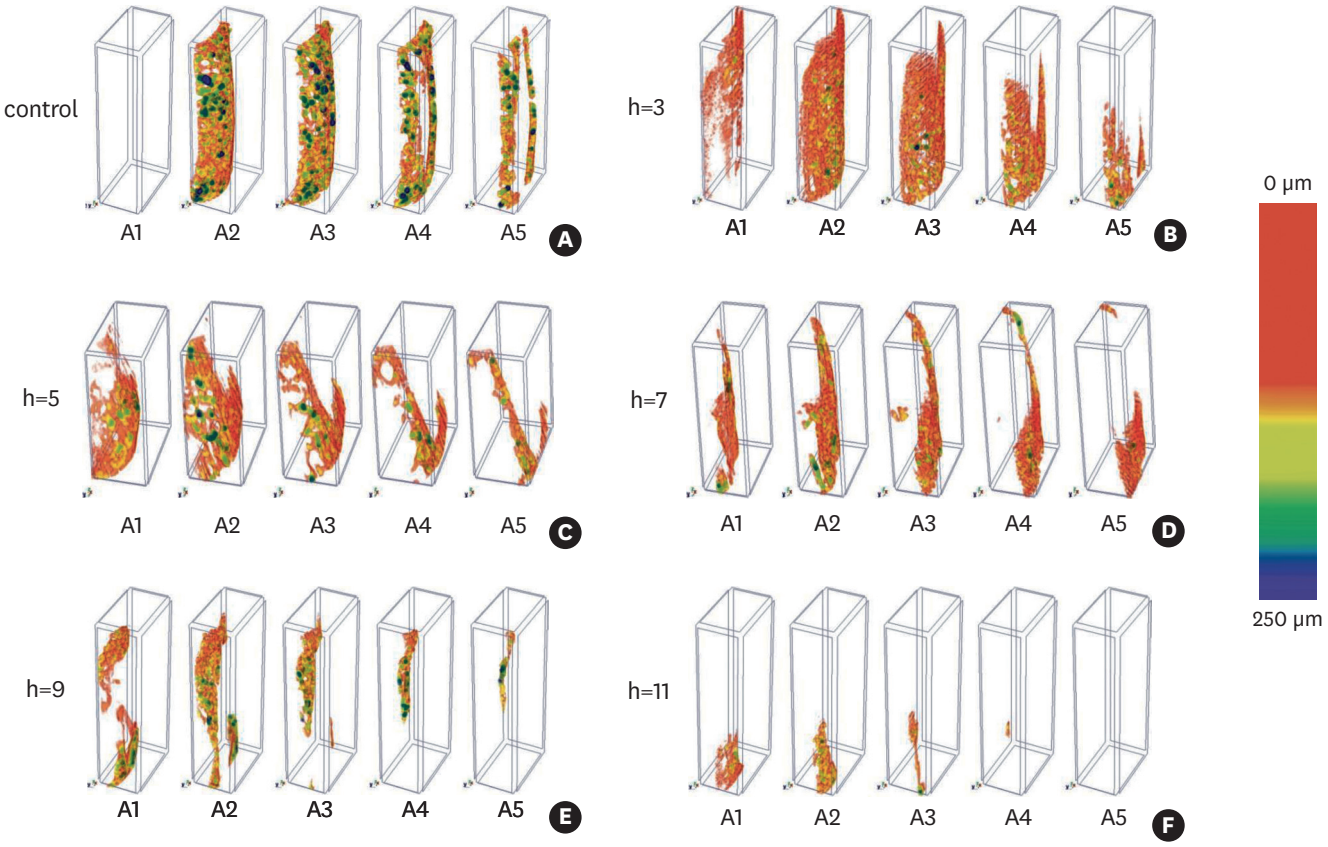

Figure 4. Color-coded trabecular thickness measured by 3-dimensional (3D) sphere fitting of alveolar bone along the entire height (h) of the defect (12 mm) but at the different area distance from the root (i.e., A1 at ≤0.4 mm, A2 at 0.4–0.8 mm, A3 at 0.8–1.2 mm, A4 at 1.2–1.6 mm, A5 at 1.6–2.0 mm). (A) Control sample; (B) sample with periodontal defect of 3 mm; (C) sample with periodontal defect of 5 mm; (D) sample with periodontal defect of 7 mm; (E) sample with periodontal defect of 9 mm; (F) sample with periodontal defect of 11 mm. The colorcoded bar is encoded between 0 and 250 μm of thickness.

instance, except for the tooth with an 11-mm defect, which exhibited resorption along the root, coronal, and medial thirds, the teeth with defects of 5 mm, 7 mm, and 9 mm exhibited more resorption in the medial third. Moreover, 2 specimens (3 mm and 7 mm) exhibited a localized area where new bone was in direct contact with the root surface (Figure 6). In addition to the details of the ankyloses, Figure 6 shows 2-dimensional tomographic sections of the alveolar bone-root interface highlighting the areas of RR. Three-dimensional models of the third mandibular incisors looking down from above illustrate the bone and root event from a macro point of view. Bone crest resorption was always observed, and this feature was prevalent in deeper defects.

Sample size

By using the value of BV/TV (%) of each area except A1 as the main outcome, the minimum within-animal difference was computed inside each area considering the differences between the BV/TV value observed in the control and those observed at each defect depth (Table 4). Standard deviations of the within-animal difference were computed for each area for all defects, excluding the control.

https://doi.org/10.5051/jpis.2016.46.5.303

JPIS
Journal of Periodontal & Implant Science

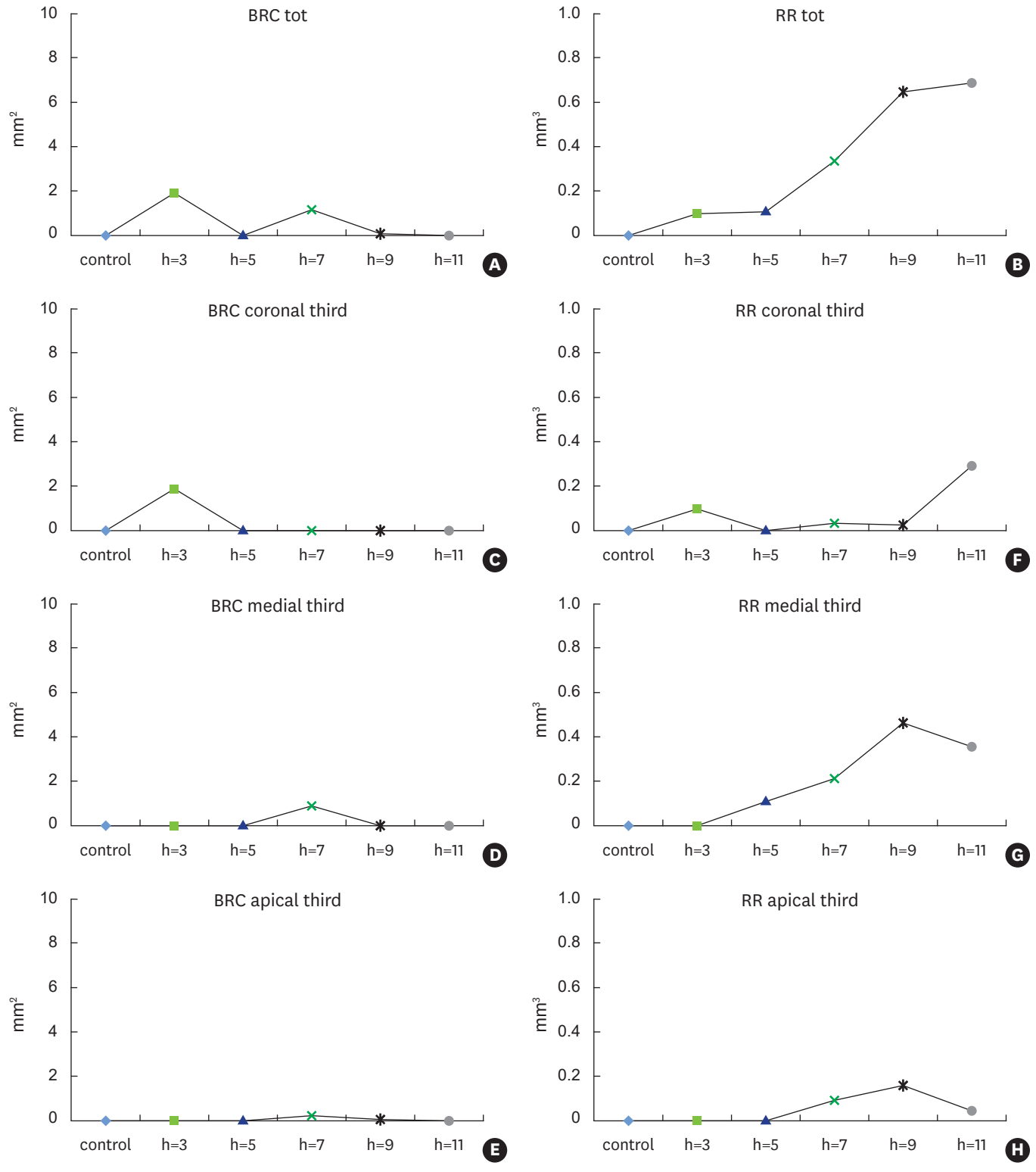

Figure 5. Bone-root contact (BRC) and root resorption (RR), in mm^2 and mm^3 respectively, of control and experimental samples. (A, B) Values of BRC and RR along the entire height (h) of the defect (12 mm). (C-H) Values of BRC and RR divided for thirds (coronal, medial, and apical).

https://doi.org/10.5051/jpis.2016.46.5.303

JPIS
Journal of Periodontal & Implant Science

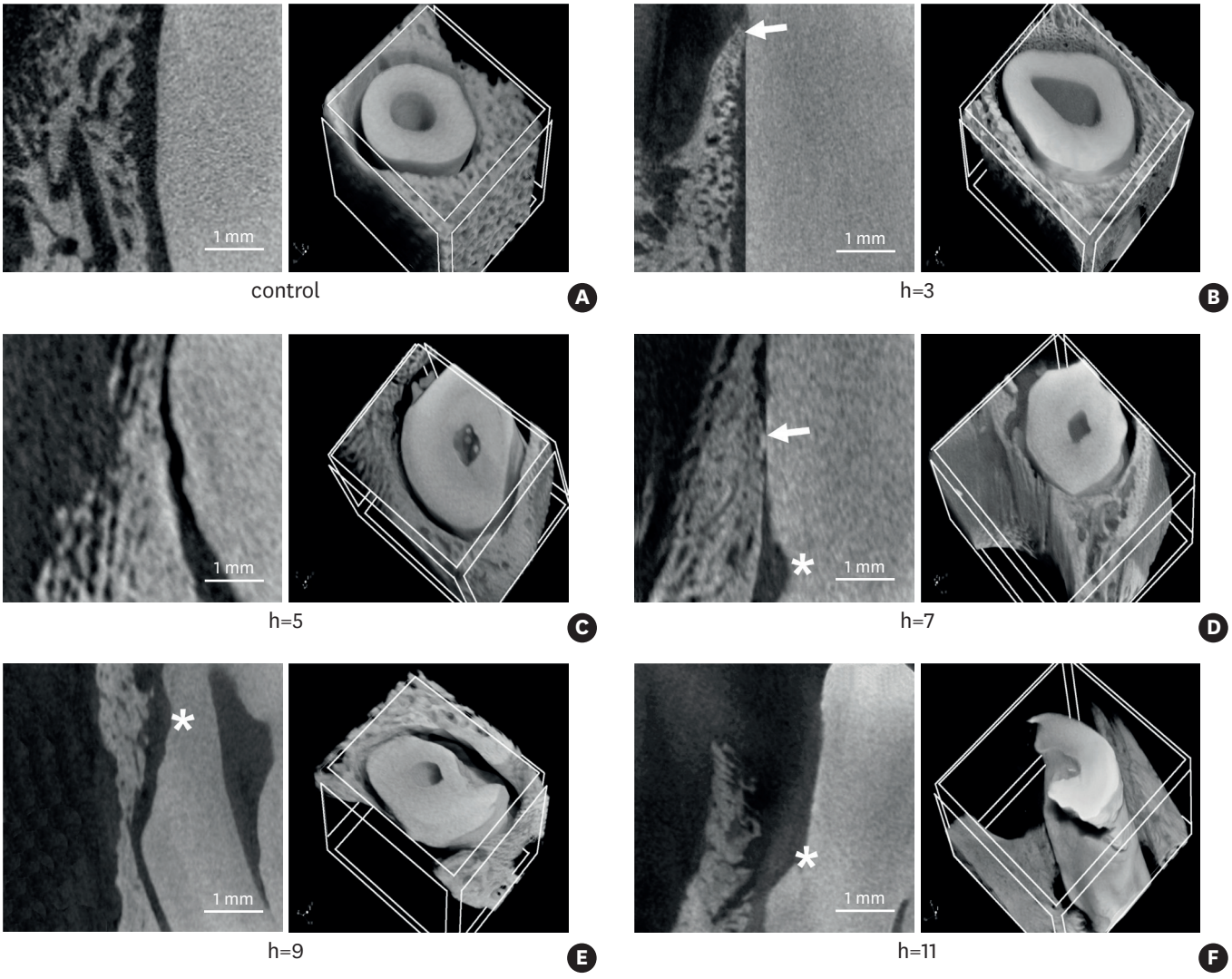

Figure 6. 2-dimensional (2D) tomographic sections and 3-dimensional (3D) models of the third mandibular incisors with gradually increasing periodontal defects. (A) Longitudinal section detail (on the left) and 3D model (on the right) of the control sample. (B) Longitudinal section detail (on the left) and 3D model (on the right) of the sample with defect depth of 3 mm showing the contact between root and alveolar bone (arrow). (C) Longitudinal section detail (on the left) and 3D model (on the right) of the sample with defect depth of 5 mm. (D) Longitudinal section detail (on the left) and 3D model (on the right) of the sample with defect depth of 7 mm showing both ankyloses (arrow). (E) Longitudinal section detail (on the left) and 3D model (on the right) of the sample with defect depth of 9 mm. (F) Longitudinal section detail (on the left) and 3D model (on the right) of the sample with defect depth of 11 mm.

h, height.

*Root resorption.

Table 4. Exact sample sizes by area

Area	Standard deviation of within-animal difference	Minimum within-animal difference	Sample size (No. of defects)	Sample size (No. of animals)
A2	0.19	0.10	28	14
A3	0.18	0.14	13	7
A4	0.13	0.08	21	11
A5	0.07	0.04	24	12

https://doi.org/10.5051/jpis.2016.46.5.303

DISCUSSION

The results of the present study confirm that, after 6 months of healing, new alveolar bone formed when dentogingival epithelium and connective tissue were prevented from interfering with the process.

The bone regrowth was greater in smaller bone defects and prevalent in the areas closest to the root surface. BV/TV, Tb.Th, and Tb.N significantly increased with decreasing defect depth, while Tb.Sp decreased, both in the tooth overall and in the coronal third. BV/TV, Tb.Sp, and Tb.N were higher in A2, A3, and A4 than in A5, both in the tooth overall and in the coronal third.

In all samples, newly formed bone around the root surface up to 1.2 mm was always detected, including the ligament space (A1, ≤0.4 mm).

The limited neo-apposition of bone in the areas further from the root surface can be explained by bone resorption of the most coronal part of the alveolar crest. The experimental model, in which full-thickness flaps were raised and wide circumferential bone defects were created, certainly induced an impairment of the vascular supply, potentially resulting in bone resorption. This was particularly true for deeper defects, where the most coronal part of the bone was more prone to suffer from these alterations.

The better regenerative healing of smaller defects that we observed is in contrast to the concepts underlying periodontal regenerative surgery, where deep intrabony defects are considered to be the best candidates [24]. This can be explained by reference to the morphology of the experimental defect. In and of itself, a circumferential shape is the worst scenario for periodontal regeneration of an intrabony defect [3]. In this morphological variant, the periodontal ligament is located only at the bottom of the defect and consequently, the deeper the preparation, the higher the distance for periodontal cells to cover. The interaction among bone and the periodontal ligament was consequently impaired in deeper defects.

Clear signs of RR in the coronal-medial areas were observed, especially in deeper defects. This observation likely indicates that tissues deriving from other sources than the periodontal ligament invaded the wound adjacent to this part of the root [6,25-27]. Since a GTR setup was used to exclude the epithelium and gingival connective tissue, alveolar bone probably dominated the wound healing process. As clearly shown in previous experimental studies in which planed dental roots were transplanted into bone and gingival connective tissue [6,25,26], resorption and ankylosis are consistent results of healing in areas directly facing the bone. Interestingly, in an animal study of repairs following the treatment of circumferential periodontal defects with barrier membranes, Crigger et al. [28] found that root surfaces were often associated with a layer of ankylosis. The authors of that study suggested that the magnitude and rate of the overall healing response exceeded the capacity of cellular elements that would lead to the regeneration of a functioning periodontium. Moreover, in a similar model, Klinge et al. [29] reported that as the size of the defect increased, creating a greater distance for proliferating cells to migrate, a concomitant increase in the frequency of ankylosis was observed.

It can be concluded that the probable absence of repopulation of the exposed root dentine by cells from the periodontal ligament may not have prevented other cells from reaching contact with the root [30].

https://doi.org/10.5051/jpis.2016.46.5.303

Based on an analysis of distribution of BRC and RR along the 3 vertical tooth axis areas, a peculiar localization can be suggested for these 2 parameters. Ankyloses were mainly localized in the coronal part of the experimental defects, while RR was observed in the medial third. However, the sample size limits the generalizability of this observation.

Higher BV/TV values were recorded in A2 (0.4–0.8 mm) for all samples. This area corresponds to the cribriform plate, also known as the bundle bone or the alveolar bone proper, which can be described as a compact layer of bone lining the tooth socket. It can be supposed that in all samples, the healing process reflected an attempt to re-form a functional periodontal anatomy.

Furthermore, high values, close to those of the control sample, were present in the apical third in the defects up to 7 mm, where the bone anatomy was less impaired by the experimental model.

In fact, observing the trends in BV/TV according to tooth anatomy, the area of the cribriform plate (A2) may have been the most affected by the defect depth. This area most likely requires more time and biomechanical load to reach its typical compact bone structure.

The Tb.Th values of the experimental defects were generally lower than that of the control and were similar among each other, independently of the distance from the root surface and the defect depth. The Tb.N and Tb.Sp values confirm the explanations presented above; in fact, the correlation of BV/TV values with similar Tb.Th values suggests the observed tendency of Tb.N and Tb.Sp to be similar.

Interestingly, the Tb.Sp in A2 was inversely correlated to the defect depth, which suggests that deeper defects probably encounter more difficulties in reconstructing the natural anatomy.

The microstructural observations showed that after 6 months of healing, the alveolar bone still displayed an immature aspect in comparison to the normal anatomy. Therefore, further bone maturation may be expected after 6 months. However, the absence of functional stimuli on the studied teeth may have affected the bone maturation process.

In the present study, signs of RR were recorded in all samples except for the control. GTR consequently failed to induce a clear regeneration in all experimental defects. Again, the fact that the experimental teeth deprived of the coronal portion were excluded from any mechanical function can be supposed to be a possible influence on the healing process. This consideration is supported by observations of the effect of splinting upon periodontal healing after replantation of permanent teeth [31-34]. Those studies observed a significant tendency for ankylosis when an extended and rigid fixation was used instead of a flexible one. Some of those authors proposed that the ingrowth of new vessels was improved by small movements during the function of the transplanted tooth, and that rigid fixations exerted a negative influence by inhibiting the mobility of the transplant [33]. Based on these considerations, it can be supposed that the total absence of a biomechanical function exerted a negative role on periodontal regeneration in the present study.

Generally, micro-CT is a non-destructive and extremely precise procedure that allows measurements of mineralized tissues, enabling the 3D evaluation of biomechanics and hard tissue healing. Another relevant advantage of this non-destructive examination method

https://doi.org/10.5051/jpis.2016.46.5.303

is the preservation of the specimen for subsequent histomorphometric analysis [35]. This volumetric technique has already been successfully applied in periodontal research, demonstrating its accuracy in the evaluation of hard tissues in cases of non-disease, disease, and healing processes [36,37]. More relevantly for this study, the application of micro-CT allowed an evaluation of the alveolar bone and root through 3D reconstruction in the axial, sagittal, and coronal planes, thereby enabling a clear view of the resorption or ankylosis location along the root, determination of the extent of tooth damage, and evaluation of bone healing. Moreover, in this paper, two new parameters (BRC and RR) were defined. These were directly derived from histomorphometric parameters widely used in the field of osseointegration; namely, bone-implant contact and bone-implant volume, respectively [38]. The possibility of standardizing the measurements, due to the removal of the operator dependence in identifying the VOIs, allowed a more accurate and reliable comparison among the values of these parameters. It is important to realize that RR manifesting as ankylosis is not evenly distributed on the root surface, and that sections obtained in different directions, typical of more conventional histomorphometric analyses, may not show the same percentage of resorption. Additionally, in order to discriminate the periodontal ligament from radiolucent areas of a different histologic origin, before evaluating the position and the volume of bone regrowth, the average size of the periodontal space was calculated. This method enabled the micro-CT assessment of resorption and ankylosis in all sample teeth.

In the present study, piezo-technology was considered the preferred method to create the experimental defects for 2 main reasons. The first was the intention to limit the side effect of bone trauma. This technology, in comparison to more conventional rotary burs, has clearly been shown to result in less damage to bone tissue and a better healing process [39]. The other reason was the calibrated diameters and the depth-dots of the inserts. These aspects, associated with good handle control and excellent visibility during use, enhanced our observations of the geometry of the experimental model.

A periodontal defect derived from periodontal disease has a different healing capability from that of an artificial defect induced by a surgical procedure [40]. This aspect can be considered a limit of the present work, but the dimensional parameters incorporated as a primary goal of the investigation imposed stringent controls on the defect shape.

Another limitation of the present work is its sample size, which is a consequence of the absence of similar investigations or previous useful data. However, as a preliminary study, it offers the opportunity to identify the optimal sample size for future investigations, which should include at least 14 animals.

Within the limits of this study, we confirmed the suggestions of the seminal 1984 study of Karring et al. [6]. In particular, in order to obtain a new fibrous attachment without the hazard of producing RR, not only the epithelium and gingival connective tissue must be prevented from interfering with healing, but bone granulation tissue should also be prevented from reaching contact with the planed root surface.

Finally, it can be concluded that this experimental model, by rejecting the null hypothesis, has provided evidence for a sort of competitive role between the periodontal ligament and alveolar bone, where the distance to the root surface seems to be the main determinant of the healing outcome.

https://doi.org/10.5051/jpis.2016.46.5.303

REFERENCES

1. Cortellini P, Bowers GM. Periodontal regeneration of intrabony defects: an evidence-based treatment approach. Int J Periodontics Restorative Dent 1995;15:128-45.
PUBMED
2. American Academy of Periodontology. Glossary of periodontal terms. 4th ed. Chicago (IL): American Academy of Periodontology; 2001.
3. Wikesjö UM, Selvig KA. Periodontal wound healing and regeneration. Periodontol 2000 1999;19:21-39.
PUBMED | CROSSREF
4. Sculean A, Nikolidakis D, Schwarz F. Regeneration of periodontal tissues: combinations of barrier membranes and grafting materials-biological foundation and preclinical evidence: a systematic review. J Clin Periodontol 2008;35:106-16.
PUBMED | CROSSREF
5. Trombelli L. Which reconstructive procedures are effective for treating the periodontal intraosseous defect? Periodontol 2000 2005;37:88-105.
PUBMED | CROSSREF
6. Karring T, Nyman S, Lindhe J, Sirirat M. Potentials for root resorption during periodontal wound healing. J Clin Periodontol 1984;11:41-52.
PUBMED | CROSSREF
7. Melcher AH. On the repair potential of periodontal tissues. J Periodontol 1976;47:256-60.
PUBMED | CROSSREF
8. Magnusson I, Claffey N, Bogle G, Garrett S, Egelberg J. Root resorption following periodontal flap procedures in monkeys. J Periodontal Res 1985;20:79-85.
PUBMED | CROSSREF
9. Klinge B, Nilvéus R, Egelberg J. Bone regeneration pattern and ankylosis in experimental furcation defects in dogs. J Clin Periodontol 1985;12:456-64.
PUBMED | CROSSREF
10. Seo BM, Miura M, Gronthos S, Bartold PM, Batouli S, Brahim J, et al. Investigation of multipotent postnatal stem cells from human periodontal ligament. Lancet 2004;364:149-55.
PUBMED | CROSSREF
11. Nagatomo K, Komaki M, Sekiya I, Sakaguchi Y, Noguchi K, Oda S, et al. Stem cell properties of human periodontal ligament cells. J Periodontal Res 2006;41:303-10.
PUBMED | CROSSREF
12. Listgarten MA, Rosenberg MM. Histological study of repair following new attachment procedures in human periodontal lesions. J Periodontol 1979;50:333-44.
PUBMED | CROSSREF
13. Linghorne WJ, O'Connell DC. Studies in the regeneration and reattachment of supporting structures of the teeth; soft tissue reattachment. J Dent Res 1950;29:419-28.
PUBMED | CROSSREF
14. Karring T, Nyman S, Gottlow J, Laurell L. Development of the biological concept of guided tissue regeneration-animal and human studies. Periodontol 2000 1993;1:26-35.
CROSSREF
15. Karring T, Cortellini P. Regenerative therapy: furcation defects. Periodontol 2000 1999;19:115-37.
PUBMED | CROSSREF
16. Polimeni G, Susin C, Wikesjö UM. Regenerative potential and healing dynamics of the periodontium: a critical-size supra-alveolar periodontal defect study. J Clin Periodontol 2009;36:258-64.
PUBMED | CROSSREF
17. Graziani F, Laurell L, Tonetti M, Gottlow J, Berglundh T. Periodontal wound healing following GTR therapy of dehiscence-type defects in the monkey: short-, medium- and long-term healing. J Clin Periodontol 2005;32:905-14.
PUBMED | CROSSREF
18. Laurell L, Bose M, Graziani F, Tonetti M, Berglundh T. The structure of periodontal tissues formed following guided tissue regeneration therapy of intra-bony defects in the monkey. J Clin Periodontol 2006;33:596-603.
PUBMED | CROSSREF
19. Samuel JL, Woodall PF. Periodontal disease in feral pigs (Sus scrofa) from Queensland, Australia. J Wildl Dis 1988;24:201-6.
PUBMED | CROSSREF

20. Štembírek J, Kyllar M, Putnová I, Stehlík L, Buchtová M. The pig as an experimental model for clinical craniofacial research. Lab Anim 2012;46:269-79.
PUBMED | CROSSREF

21. Hildebrand T, Rüegsegger P. Quantification of bone microarchitecture with the structure model index. Comput Methods Biomech Biomed Engin 1997;1:15-23.

22. Russell WM, Burch RL. The principles of humane experimental technique [Internet]. Baltimore (MD): Johns Hopkins University; [cited 2015 Jun 24]. Available from: http://altweb.jhsph.edu/pubs/books/humane_exp/het-toc.

23. Pandis N. Sample calculation for split-mouth designs. Am J Orthod Dentofacial Orthop 2012;141:818-9.
PUBMED | CROSSREF

24. Becker W, Becker BE. Periodontal regeneration: a contemporary re-evaluation. Periodontol 2000 1999;19:104-14.
PUBMED | CROSSREF

25. Karring T, Nyman S, Lindhe J. Healing following implantation of periodontitis affected roots into bone tissue. J Clin Periodontol 1980;7:96-105.
PUBMED | CROSSREF

26. Nyman S, Karring T, Lindhe J, Plantén S. Healing following implantation of periodontitis-affected roots into gingival connective tissue. J Clin Periodontol 1980;7:394-401.
PUBMED | CROSSREF

27. Gottlow J, Nyman S, Karring T. Healing following citric acid conditioning of roots implanted into bone and gingival connective tissue. J Periodontal Res 1984;19:214-20.
PUBMED | CROSSREF

28. Crigger M, Bogle GC, Garrett S, Gantes BG. Repair following treatment of circumferential periodontal defects in dogs with collagen and expanded polytetrafluoroethylene barrier membranes. J Periodontol 1996;67:403-13.
PUBMED | CROSSREF

29. Klinge B, Nilvéus R, Kiger RD, Egelberg J. Effect of flap placement and defect size on healing of experimental furcation defects. J Periodontal Res 1981;16:236-48.
PUBMED | CROSSREF

30. Karring T, Isidor F, Nyman S, Lindhe J. New attachment formation on teeth with a reduced but healthy periodontal ligament. J Clin Periodontol 1985;12:51-60.
PUBMED | CROSSREF

31. Andreasen JO. The effect of splinting upon periodontal healing after replantation of permanent incisors in monkeys. Acta Odontol Scand 1975;33:313-23.
CROSSREF

32. Nasjleti CE, Castelli WA, Caffesse RG. The effects of different splinting times on replantation of teeth in monkeys. Oral Surg Oral Med Oral Pathol 1982;53:557-66.
PUBMED | CROSSREF

33. Kristerson L, Andreasen JO. The effect of splinting upon periodontal and pulpal healing after autotransplantation of mature and immature permanent incisors in monkeys. Int J Oral Surg 1983;12:239-49.
PUBMED | CROSSREF

34. Bauss O, Schilke R, Fenske C, Engelke W, Kiliaridis S. Autotransplantation of immature third molars: influence of different splinting methods and fixation periods. Dent Traumatol 2002;18:322-8.
PUBMED | CROSSREF

35. Gandolfi MG, Parrilli AP, Fini M, Prati C, Dummer PM. 3D micro-CT analysis of the interface voids associated with Thermafil root fillings used with AH Plus or a flowable MTA sealer. Int Endod J 2013;46:253-63.
PUBMED | CROSSREF

36. Park CH, Abramson ZR, Taba M Jr, Jin Q, Chang J, Kreider JM, et al. Three-dimensional micro-computed tomographic imaging of alveolar bone in experimental bone loss or repair. J Periodontol 2007;78:273-81.
PUBMED | CROSSREF

37. de Paula Reis MV, Moura CC, Soares PB, Leoni GB, Souza-Neto MD, Barbosa DZ, et al. Histologic and micro-computed tomographic analyses of replanted teeth stored in different kind of media. J Endod 2014;40:665-9.
PUBMED | CROSSREF

38. Martini L, Staffa G, Giavaresi G, Salamanna F, Parrilli A, Serchi E, et al. Long-term results following cranial hydroxyapatite prosthesis implantation in a large skull defect model. Plast Reconstr Surg 2012;129:625e-635e.
PUBMED | CROSSREF

39. Vercellotti T, Nevins ML, Kim DM, Nevins M, Wada K, Schenk RK, et al. Osseous response following resective therapy with piezosurgery. Int J Periodontics Restorative Dent 2005;25:543-9.
PUBMED

40. Do MJ, Kim K, Lee H, Cha S, Seo T, Park HJ, et al. Development of animal experimental periodontitis models. J Periodontal Implant Sci 2013;43:147-52.
PUBMED | CROSSREF